Cell competition confers anchorage plasticity of disseminated tumor cells

Hyunbin D. Huh[1]†, Yujin Sub[2]†, Jee Hung Kim[3,4], Hannah Lee[1], Jongwook Oh[2], Dong Ki Lee[3], Jong Hwa Byun[1], Woo Yang Pyun[1], Sehyung Pak[5], Junjeong Choi[6], Joon Jeong[3,4]*, Heon Yung Gee[2]*, and Hyun Woo Park[1]*

[1] Department of Biochemistry, College of Life Science and Biotechnology, Brain Korea 21 Project, Yonsei University; Seoul 03722, Republic of Korea.

[2] Department of Pharmacology, Graduate School of Medical Science, Brain Korea 21 Project, Yonsei University College of Medicine; Seoul 03722, Republic of Korea.

[3] Division of Medical Oncology, Department of Internal Medicine, Gangnam Severance Hospital, Yonsei University College of Medicine, Seoul, Korea.

[4] Institute for Breast Cancer Precision Medicine, Yonsei University College of Medicine, Seoul, Republic of Korea.

[5] Cytogen, Seoul, Republic of Korea

[6] College of Pharmacy, Yonsei Institute of Pharmaceutical Sciences, Yonsei University, Incheon, Republic of Korea.

† Equal contributions

*Corresponding authors. Email: Hyun Woo Park (hwp003@yonsei.ac.kr), Heon Yung Gee (hygee@yuhs.ac), Joon Jeong (gsjjoon@yuhs.ac)

Abstract

Cell competition within the primary tumor drives tumor growth by promoting the uncontrolled proliferation of winner cells and eliminating loser cells by sensing cell fitness. However, the mechanism how cell competition confers loser cells with the metastatic potential of circulating tumor cells (CTCs) remains elusive. Unexpectedly, we found cell competition-induced less fit but viable cells transformed into CTCs via adherent-to-suspension transition (AST) mechanisms in dissemination assay. The induction of AST factors, hematopoietic transcription factors hijacked by solid tumor cells, rendered CTCs competent to lose anchorage dependency and disseminate into the bloodstream, while subsequent suppression of these factors in CTCs was critical to regain adhesion and colonize metastatic lesions. Disrupting the oscillatory dynamics of AST factors blocked the adherent-suspension plasticity (ASP) of breast cancer CTCs and suppressed lung metastasis. Furthermore, multiregional single-cell transcriptomic analyses of matched primary tumors, CTCs, and metastatic lesions from *de novo* metastatic breast cancer patients identified the critical role of ASP in metastasis.

Significance

We demonstrate that cell competition-mediated displacement of CTCs manifests dynamic oscillation of AST factors that confer anchorage plasticity of solid tumor cells critical for the dissemination and colonization of CTCs. These findings highlight the potential of targeting AST factors to develop effective anti-metastatic therapies.

42 ## Introduction

43 Multicellular development is characterized by competitive cells outcompeting less fit cells,
44 which are programmed to disappear in order to maintain homeostasis, thereby ensuring the
45 functional and structural integrity of tissues. This cell fitness monitoring system, known as 'cell
46 competition', occurs through mechanical competition that depend on cell-cell interactions or
47 molecular competition driven by soluble factors secreted by neighboring cells. In cancer, where
48 genetic heterogeneity plays a significant role, cell competition exerts various pressures on
49 tumorigenesis. Competitive intratumoral cells can influence tumor malignancy through clonal
50 expansion, while less fit cells that detach from the parental cell population may contribute to cancer
51 metastasis. Metastatic dissemination of primary tumor cells requires the detachment of circulating
52 tumor cells (CTCs) into the lymphatic or blood microvasculature, resist anoikis while migrating
53 through the bloodstream, and adapt to foreign microenvironment in distant tissues [1, 2]. However,
54 the physiological similarity between less-fit cells detached from the primary tumor through cell
55 competition and CTCs remains to be clarified.

56 The metastatic cascade could be perceived as a consequence of cancer cells constantly
57 transitioning between an adherent state and a suspension state [3]. We recently discovered a
58 biological phenomenon, adherent-to-suspension transition (AST), a mechanism that reprograms
59 the anchorage dependency of solid tumor cells via hematopoietic transcription factors termed AST
60 factors to facilitate the dissemination and release of circulating tumor cells (CTCs) [4-6]. Despite
61 the absence of lineage differentiation and EMT (epithelial-to-mesenchymal transition), the
62 induction of AST in solid tumor cells 1) suppresses global integrin/extracellular matrix (ECM)
63 gene expression via YAP-TEAD inhibition to evoke spontaneous cell-matrix dissociation and 2)
64 upregulates globin genes to prevent oxidative stress and permit the acquisition of anoikis

65 resistance. Once in the bloodstream, the resulting CTCs could reattach and colonize distant organs
66 to initiate metastatic outgrowth [7]. It remains unclear, however, whether the regulation of CTC
67 anchorage dependency throughout the metastatic cascade requires dynamic plasticity in AST
68 factor expression.

69 Previously, we observed in mice an induction of AST factors during melanoma CTC
70 dissemination and a subsequent reduction of these factors in colonized lung nodules to levels
71 resembling those of primary tumor cells, suggesting that AST factor expression can show
72 reversible plasticity [4]. In addition, when we triggered a transient induction and reduction of
73 ectopically expressed AST factors, we observed a strong correlation with the loss and gain of
74 anchorage dependency. Although it remains unclear whether these plastic changes in AST
75 expression are important for human cancer metastasis, the direct correlation we observed between
76 AST factor oscillation and the reprogramming of anchorage dependency led us to pursue the
77 hypothesis that the dynamic spatiotemporal modulation of AST factor expression is crucial for the
78 spontaneous dissemination and colonization of CTCs during metastatic outgrowth.

79 To investigate adherent-suspension plasticity in cancer patients, we established a
80 comprehensive biobank and analyzed the alteration of AST factor expression during the
81 dissemination and colonization of CTCs. We enrolled untreated *de novo* metastatic breast cancer
82 patients and analyzed single-cell level transcriptomes of matched tissue and liquid biopsy
83 specimens comprising 1) primary tumors, 2) CTCs, and 3) metastatic lesions. To date, most
84 transcriptomic studies in cancer patients seeking to uncover the molecular mechanisms of
85 metastasis have focused on individual analyses of either primary tumors, CTCs, or metastatic
86 lesions. There have also been analyses comparing primary tumors with CTCs or metastatic lesions
87 from unrelated patients [13-17]. To monitor the dynamic plasticity of AST factors and related gene

88 signatures that encompass the metastatic cascade from dissemination to colonization, we have
89 demonstrated the necessity of comparing the transcriptomes of CTCs with the transcriptomes of
90 matched solid tumor counterparts derived from the same patient. Thus, performing a cell
91 competition assay and analyzing single-cell-level transcriptomes of matched specimens from *de*
92 *novo* metastatic breast cancer patients, our study has revealed how anchorage plasticity drives the
93 metastatic cascade in disseminated CTCs via AST factor-mediated ASP.
94

95 ## Results

96 **Cell competiton orchestrates spontaneous detachment of CTC-like cells driven by AST**
97 **factors expression *in vitro.***

98 Malignant tumors are characterized by the mobilization of cancer cells that have lost
99 contact inhibition of proliferation (CIP). This leads to cell crowding-induced hostile tumor
100 microenvironment (TME) that drives dissemination of CTCs from their primary tumor into the
101 blood vessels. The metastatic cascade, therefore, could be conceived as a consequence of cancer
102 cells constantly transitioning between the adherent and suspension states. Tumors with genomic
103 and epigenomic heterogeneity acquire competitive and aggressive cancer cells through a fitness-
104 based selection mechanism of cell competition in high cell density environments. Recent studies
105 have also reported that highly metastatic cells are generated and displaced through cell competition.

106 To examine whether cell competition in a high cell density environment facilitates the
107 displacement of CTCs from parental cells, we exposed various subtypes of breast cancer cell lines,
108 including MDA-MB-231, MCF7, BT549, and Hs578T, to sustained high cell density stress
109 conditions that promote cell competition. Notably, while other breast cancer cell lines we tested
110 exhibited contact inhibition or cell death, only in MDA-MB-231 cells, cell competition results in
111 the rounding and detachment of CTC-like cancer cells that resemble the rare population of

112 disseminated CTCs *in vivo* (**Fig. 1A-B**). We hypothesized that the ability of a cell line to produce
113 CTC-like cells through cell competition would likely also reflect its metastatic capacity *in vivo*.
114 To test this, we injected each breast cancer cell line into the fat pad of mice and examined the
115 efficiency with which they disseminated to colonize the lung (**Fig. 1C**). As expected, despite
116 showing similar primary tumor growth, the cell lines that failed to generate CTC-like cells in the
117 cell competition showed significantly lower metastatic potential and permitted longer survival than
118 MDA-MB-231 (**Fig. 1D**). This observation correlates with earlier metastasis map (Metmap)
119 findings classifying MDA-MB-231 as one of the most malignant breast cancer cell lines (**Fig. S1A**)
120 [18]. Thus, these results suggests that only the most malignant breast cancer cells obtain a
121 competitive benefit in cell competition, leading to the production of spontaneously suspended
122 CTC-like cells. Next, to identify the molecular characteristics of cellular displacement of CTC-
123 like cells, we collected suspended CTC-like cells and adherent parental cells for single-cell RNA
124 sequencing analysis (**Fig. 1E-F**). Interestingly, GSEA analysis revealed that parental cells
125 exhibited significant enrichment in gene sets associated with cell-matrix adhesion, positive
126 regulation of substrate adhesion-dependent cell spreading, and positive regulation of stress fiber
127 assembly compared to CTC-like cells. These findings indicate that CTC-like cells are defined by
128 the active downregulation of anchorage dependency. (**Fig. 1G**). This prompted us to investigate
129 the downregulated genes associated with the ability of CTC-like cells to adhere to the extracellular
130 matrix. Notably, CTC-like cells exhibited a significant reduction in the expression of genes
131 involved in focal adhesion formation, a process essential for cancer cells to retain their adherent
132 properties as part of a primary tumor (**Fig. 1H**). These results suggest that cell competition drives
133 the displacement of cells that have been reprogrammed to undergo spontaneous detachment (**Fig.
134 1I**). Recent reports have demonstrated that heterogeneity in the expression and activity of YAP1

135 and TEAD in cancer enables YAP^{hi} and $TEAD^{hi}$ cells, which are more competitive in resisting
136 mechanical pressures, to outcompete YAP^{low} and $TEAD^{low}$ cells, thereby conferring a growth
137 advantage to the tumor. Moreover, Hippo pathway has been shown to promote cell-matrix
138 dissociation, facilitating the detachment of cancer cells from the primary tumor. Interestingly, we
139 discovered that gene sets associated with Hippo signaling were enriched specifically in parental
140 cells (**Fig. 1J**). Additionally, the expression of core mediators of the Hippo pathway was
141 specifically reduced in CTC-like cells (**Fig. 1K**). Given our previous findings that cancer cells lose
142 anchorage dependency through adherent-to-suspension transition (AST)-mediated reduction in
143 TEAD expression and YAP inactivation, we sought to investigate whether the formation of CTC-
144 like cells occurs via the AST. We were surprised to find that CTC-like cells population
145 recapitulated the aberrant induction of endogenous AST factors, which were highly elevated in
146 CTCs derived from mouse models and *de novo* metastatic breast cancer patients. Detached CTC-
147 like MDA-MB-231 cells showed much higher levels of the AST factors, including NFE2, BTG2,
148 IRF8 and IKZF1, than their adhesive counterparts that mirrored the primary tumor (**Fig. 1L**).
149 Notably and in contrast to the CTC-like cells isolated from the cell competition, we found
150 significantly lower levels of these AST factors in cells harvested from suspension culture assay
151 (**Fig. S1B**). To verify whether the induction of AST factors is required for the spontaneous
152 detachment of CTC-like cells, we used siRNA to knockdown each factor and measured the
153 displacement efficiency as an indication of the viability of CTC-like cells produced in cell
154 competition. Although we previously showed that the overexpression of a combination of
155 hematopoietic factors enhanced AST efficiency [4], these knockdown experiments indicated that
156 the depletion of any single AST factor was sufficient to markedly suppress the formation of CTC-
157 like cells (**Fig. 1M**). Moreover, we found that pretreatment with thalidomide derivatives like

158 lenalidomide or pomalidomide, which we previously identified as potential anti-metastatic agents
159 that act by reducing the expression of IKZF1 in mouse breast cancer models [4], substantially
160 inhibited the production of CTC-like cells (**Fig. 1N**). These results demonstrate that AST factor
161 induction is required for the detachment and survival of CTC-like cells.
162

163 **CTC-like cells reflect CTCs characterized by AST factor expression.**

164 Next, we asked whether CTC-like cells derived *in vitro* through cell competition and *in*
165 *vivo* CTCs exhibit similar characteristics. To test this, we integrated and analyzed scRNA-seq data
166 from parental and CTC-like cells derived from a cell competition *in vitro* using the MDA-MB-
167 231-derived LM2 cell line, alongside primary tumor and CTC data from LM2 cells in a mouse
168 fatpad-to-lung metastasis *in vivo* model (**Fig. 2A**). In UMAP analysis, cells were clustered
169 according to the four sample types, as well as based on the Leiden algorithm (**Fig. 2B-C**).
170 Interestingly, while the majority of CTCs are primarily located in Leiden cluster 3, CTCs with
171 high expression levels of AST factors are predominantly clustered with the majority of the CTC-
172 like cell population in Leiden cluster 1 (**Fig. 2D-E**). This suggests that aberrant expression of AST
173 in CTCs may drive transcriptional similarities to CTC-like cells. To investigate the characteristics
174 of CTCs in cluster 1, we annotated these cells as AST^{high} CTCs (**Fig. 2F)**. Surprisingly, Pearson
175 correlation analysis of this annotated cell type revealed that *in vivo* AST^{high} CTCs, obtained from
176 the mouse metastasis model, show the highest positive transcriptomic correlation with *in vitro*
177 CTC-like cells, rather than with the primary tumor *in vivo* (**Fig. 2G)**. We also identified the top
178 five genes strongly expressed in both CTC-like cells and AST^{high} CTCs, including BTG2, RGS2,
179 NFKBIZ, IRE5, and SGK1, compared to the other cell types (**Fig. 2H-I)**. This result strongly
180 demonstrate that CTC-like cells spontaneously detached from parental cells as suspension cells

181 through cell competition physiologically recapitulate disseminated CTCs from the primary tumor
182 that have undergone AST-mediated reprogramming (**Fig. 2J**).
183

184 **CTC-like cells and CTCs confer anchorage dependency plasticity accompanied by**
185 **AST factors oscillation.**

186 Cell competition further allowed us to assessed whether the anchorage independence of
187 CTC-like cells reprogrammed by endogenous expression of AST factors is permanent or reversible.
188 When we isolated and replated the CTC-like cells to examine their anchorage plasticity, we found
189 that CTC-like cells lost their anchorage independence and readily attached to the culture dish to
190 continue proliferating as adherent cells. We refer to these newly adherent cells as met-like cells
191 because they seem to simulate the final stage of the metastatic cascade in which suspended tumor
192 cells in the circulation regain adhesive properties to reattach and colonize a secondary organ.
193 Surprisingly, we found that the met-like cells showed a significant reduction in the increased AST
194 factor expression that had promoted their spontaneous detachment as CTC-like cells, having
195 undergone the suspension-to-adherent transition (SAT) (**Fig. 3A**). These results show that AST
196 factor dynamics in CTC-like cells undergoing AST and SAT transition correlate with the
197 anchorage plasticity of solid tumor cells in a way that is quite distinct from the primary-like or
198 met-like cells. Moreover, because our results establish AST factors as mechanosensitive
199 transcription factors, the mechanisms underlying their mechanical regulation in solid tumor cells
200 warrant further investigation.

201 Proceeding from our previous results establishing the role of AST factor induction in CTC
202 dissemination, we next asked whether AST factor repression is critical for the reattachment and
203 colonization of CTCs *in vivo*. We next generated LM2-AST cells from MDA-MB-231 breast

204 cancer cells selected for its their ability to metastasize to the lung (**Fig. 3C**) [19]. In contrast to
205 control cells, LM2-AST cells stably expressing AST factors elicited spontaneous detachment and
206 anoikis resistance. To determine whether the constitutive activation of AST factors in CTCs
207 impedes lung colonization, we injected LM2-control and LM2-AST cells into the tail vein of
208 NOD/SCID gamma (NSG) mice (**Fig. 3D**). Remarkably, while the LM2-control cells produced
209 successful lung metastases, the stable expression of AST factors in LM2-AST cells dramatically
210 suppressed lung colonization and prolonged survival (**Fig. 3E-G**). This indicates that, while the
211 induction of AST factors evokes CTC dissemination, the subsequent repression of AST factors in
212 CTCs is required for colonization. Together, CTC-like cells demonstrate that AST factor
213 dynamics-their induction during the primary-to-CTC transition and their repression during the
214 CTC-to-mets transition-are critical for the dissemination and colonization of CTCs.

215 We speculated that ASP is a biologically significant process involved in dynamically
216 regulating the anchorage dependency of CTCs during metastasis *in vivo*. To assess the clinical
217 relevance of ASP in human subjects, we recruited 10 newly diagnosed *de novo* metastatic breast
218 cancer patients and collected matched samples consisting of breast primary tumors, blood cells,
219 and metastatic lesions from each patient (**Table S1**, **Fig. 3H**). Thus, our patient data provides one
220 of the most comprehensive biobanks available to date by analyzing both tissue and liquid biopsy
221 specimens compared to previous studies [13-16]. We then used high density microporous (HDM)
222 chips to enrich CTCs from whole blood via size exclusion. Isolated tissue cells and CTCs were
223 then further processed for single-cell RNA sequencing (scRNA-seq) [20]. We identified epithelial
224 cells, mesenchymal stem cells, fibroblasts, and various immune cells, such as myeloid cells and
225 lymphocytes (**Fig. S2A-B**). Within the overall cell population, we identified cancer cells as those
226 co-expressing EPCAM with the breast cancer-specific cytokeratins KRT5, KRT8, KRT9, KRT17,

227 or KRT18 (**Fig. 3I-C**, **S2A-B**). A UMAP analysis revealed a clustering of the cells based on patient
228 and tissue of origin. Interestingly, there was a mixture of cells in the center region consisted of
229 different patients and tissues, where most CTCs were also located (**Fig.3I**). Surprisingly, this
230 region showed higher expression levels of AST factors, including IKZF1, NFE2, and IRF8 (**Fig.3I**).
231 Upon further examination, we found that the expression of AST factors in CTCs greatly exceeded
232 that of either primary or metastatic tumor cells, with the levels of IKZF1 and IRF8 rising above
233 the statistical significance threshold (**Fig. 3J**, **Fig. S2C**). The increase in AST factor expression
234 was consistent regardless of breast cancer subtype or organ tropism of metastatic tumors. These
235 results demonstrate the clinical relevance of ASP in the metastatic cascade of human patients by
236 regulating the anchorage dependency of CTCs.

237 Previously, when performing a gene set enrichment analysis (GSEA) comparing primary
238 tumors and CTCs, we found significant enrichment of gene sets related to focal adhesion and ECM
239 organization [4]. We confirmed the upregulation of focal adhesion-related genes in both primary
240 tumors and metastatic lesions compared to CTCs (**Fig. S2D**) and the enrichment of ECM
241 organization pathways in metastatic tumors compared to CTCs (**Fig. S2D**). In contrast, CTCs
242 showed a significant decrease in genes related to ECM components and integrins, and a significant
243 increase in the hemoglobin genes HBA1 and HBA2, which protect CTCs against reactive oxygen
244 species (ROS)-induced anoikis (**Fig. 3J**) [4]. These findings in metastatic cancer patients
245 demonstrate that oscillatory AST factor dynamics lead to anchorage plasticity by altering gene
246 expression associated with integrin/ECM components and anoikis resistance.

247

248 **Adherent-suspension plasticity in the metastatic cascade of *de novo* metastatic**
249 **breast cancer patients**

250 Next, we analyzed the characteristics of CTCs in comparison to their solid tumor
251 counterparts. We focused on the central region of the UMAP, located at similar points in
252 pseudotime analysis (**Fig. 4A**). Cells located outside the central region of the UMAP were
253 clustered together based on cancer stage, tissue origin, and patient identity. The cancer cells were
254 divided into 25 clusters based on gene expression (**Fig. 4A**). To enrich for CTCs in the central
255 region, we considered the following factors: 1) increasing the number of CTCs and 2) enhancing
256 transcript expression similarity among cells, as indicated by a decreased standard deviation of their
257 respective UMAP1 and UMAP2 values (**Fig. S3A-B**). Based on these criteria, we chose eight
258 clusters (i.e., clusters 9, 11, 12, 13, 15, 17, 20, and 24) to represent the center region of the UMAP
259 (**Fig. 4B-F, Fig. S3A**). The center region contains 8,823 solid tumor cells, comprising 3,695
260 primary tumor cells and 5,128 metastatic cancer cells, along with 34 CTCs (**Fig. 4D**). We then
261 examined AST factor expression in cells located within the central region. Pseudotime analysis of
262 the central region clusters indicates a significant increase in AST factor expression, including
263 IKZF1 and IRF8, compared to earlier stages that then decreased again in later stages (**Fig. 4E-G**).
264 These observations suggest that the transcriptional profile of solid tumor cells from primary and
265 metastatic lesions in the central region resembles that of CTCs, indicating an intermediate state,
266 not yet fully transformed into CTCs. [8]

267 To further explore the molecular differences between CTCs and solid tumor cells, as well
268 as the mechanisms underlying the transition observed in the central region, we compared the
269 differentially expressed genes (DEGs) between the two cell types within this region (**Fig**. **4H,**
270 **S3C**), identifying 1,223 CTC-specific and 59 solid tumor-specific genes (**Fig. 4H**). By performing
271 a gene ontology (GO) analysis of the CTC-specific genes, we noticed enrichment of a gene set
272 related to rRNA processing, suggesting ribosome biogenesis is necessary for the protein synthesis

273 that facilitates CTC survival and metastatic potential (**Fig**. **4I**). Although not all superoxide
274 resistance pathways were enriched in the GO analysis, the CTCs in the central region showed
275 specific upregulation of hemoglobin gene, HBA1, which plays an antioxidant role and provides
276 cells with resistance to anoikis, enhancing their metastatic potential (**Fig**. **4J**). In contrast, GO
277 analysis of the solid tumor-specific genes revealed enrichment for terms related to cell adhesion
278 and ECM production (**Fig**. **4I**). These results highlight the distinct cellular behavior of CTCs and
279 solid tumor cells. While CTCs tend to exhibit dynamic, non-adherent properties essential for the
280 survival in circulation, solid tumor cells maintain strong adhesion to the ECM.

281 Psuedotime analysis provided further insights into this transition by revealing that while
282 most solid tumor cells did not express AST factors (AST-negative cells), some positioned at
283 pseudotime points similar to CTCs did exhibit AST factor expression (AST-positive cells) (**Fig**.
284 **4E-F**). To further investigate the differences between these AST-positive and AST-negative solid
285 tumor cells, we conducted DEG analyses comparing the corresponding primary and metastatic
286 tumors. This allowed us to identify 2,112 AST-positive-specific genes and 166 AST-negative-
287 specific genes in the primary tumors versus 1,284 AST-positive-specific genes and 213 AST-
288 negative-specific genes in the metastatic tumors (**Fig**. **4K**). Underscoring the similarity of the two
289 conditions, we found a considerable overlap of 997 AST-positive-specific genes and 45 AST-
290 negative-specific genes that were shared between the primary and metastatic tumors. A GO
291 analysis of these AST-positive-specific genes revealed enrichment in the MAPK- ERK1/2 cascade,
292 which is associated with antioxidant expression, anoikis resistance, and metalloproteinase-
293 mediated ECM degradation (**Fig**. **4L**) [21-24]. In the AST-positive cells, we also identified genes
294 related to extravasation, which suggests that, like CTCs, these cells possess increased invasive
295 properties. In contrast, GO analysis of the AST-negative-specific genes revealed enrichment in

296 pathways related to anchoring junctions, ECM, and focal adhesions, which promote cell adhesion
297 and structural integrity (**Fig**. **4L**). GSEA analysis confirmed that AST-negative cells in both
298 primary and metastatic tumors showed significant enrichment in gene sets related to tight junctions
299 and ECM organization (**Fig**. **4M**). This further supports the notion that AST-negative cells are
300 characterized by strong adhesion properties. In contrast, AST-positive cells, particularly in the
301 central region, co-expressed genes involved in the MAPK cascade, ERK1/2 cascade, and
302 extravasation. Thus, some solid tumor cells exhibit an expression pattern like that of CTCs,
303 indicating the presence of cells with CTC-like characteristics within the solid tumor population.
304 Finally, we analyzed RNA velocity to clarify the correlation of AST factor expression
305 dynamics with the expression of integrin/ECM-related, antioxidant-related, and EMT-related
306 genes (**Fig. 4F, S3D**). Although we found no correlation between AST factors and EMT-related
307 genes, there was a correlation between EMT-related genes and ECM-related genes, which
308 correlates with our previous study that AST is independent of EMT.
309

310 ## Discussion

311 Cell competition in tumors is a system that leverages the heterogeneity of cancer cells in
312 stressful microenvironments, such as high cell density, to select for cells that contribute to tumor
313 survival and progression. During this process, less fit cells either undergo apoptosis or detach from
314 the existing colonies. Recent studies have indicated that cells with metastatic traits can lose their
315 competitive advantage within primary tumors and detach. In our study, we found that cells
316 detached from the primary tumor due to cell competition acquire anchorage independence via AST
317 factors, and are transcriptionally similar to circulating tumor cells (CTCs) expressing AST factors.
318 This suggests the potential for conducting in vitro studies on CTCs using cell competition assays

319 with metastatic cells. Previous attempts have aimed to study CTCs at the molecular level in vitro,
320 including efforts to establish ex vivo CTC cell lines from patient samples. Furthermore, suspension
321 assays, which assess anchorage-independent growth, have been widely used to investigate the
322 anoikis resistance of CTCs. However, because this assay use trypsinized cells, they cannot mimic
323 the spontaneous process by which CTCs disseminate *in vivo*, nor can they generate the exceedingly
324 rare population of CTC-like cells that can freely detach from adherent culture conditions.
325 Therefore, the CTC-like cells identified through cell competition will shed light on the overall
326 understanding of the mechanical modulation involved in the dissemination and survival of AST-
327 associated CTCs, paving the way for the discovery of potential anti-metastatic agents.

328 Our study highlights the need to distinguish anti-metastatic strategies from traditional
329 cancer therapies that promote competitive cells towards a less fit direction within the primary
330 tumor's cell competition context. For instance, cancer therapies targeting Hippo pathway effector
331 proteins such as TEAD or YAP suppress tumor proliferation by inhibiting the competitive
332 advantage of YAP^{hi} or $TEAD^{hi}$ cells. However, based on our findings that less fit CTC-like cells
333 or CTCs dissociated from the parental population are $TEAD^{low}$, targeting TEAD could
334 inadvertently increase the less fit cell population, potentially promoting metastasis. Therefore,
335 anti-cancer therapies and anti-metastatic agents should be developed with a more nuanced
336 understanding of how shifts in the dominance between competitive and less fit cells in the context
337 of cell competition within primary tumors can influence tumorigenesis and metastasis, respectively.
338 This approach would ensure that anti-cancer therapies do not inadvertently promote metastasis,
339 and anti-metastatic agents do not compromise tumor progression.

340 We demonstrated that, while AST factors facilitate the initial detachment and anoikis
341 resistance of CTC-like cells, their downregulation is essential for the reattachment and successful

342 colonization of cancer cells at distant metastatic sites. This indicates that metastatic success
343 depends on the ability of cancer cells to adapt their anchorage dependency to each stage of
344 metastasis. Suspension characteristics mobilize CTCs into the bloodstream, whereas reattachment
345 and colony formation necessitate a reversion to adherent traits within the microenvironment of
346 secondary sites. These insights challenge the conventional understanding of metastasis as a linear
347 progression and instead propose a model in which anchorage plasticity plays a central role in
348 cancer cells to spread during metastasis. ASP thus represents a novel cellular plasticity mechanism
349 analogous to epithelial-mesenchymal plasticity (EMP), another well-established process that
350 facilitates metastasis, however, limited to the transition between two different adhesive cell types.
351 How cancer cells orchestrate ASP and EMP during each stage of the metastatic cascade warrants
352 further investigation.

353 Our findings underscore the pivotal role of ASP in the metastatic cascade, as demonstrated
354 by scRNA-seq analysis of paired samples from *de novo* metastatic breast cancer patients,
355 encompassing matched primary tumors, CTCs, and metastatic lesions. This dataset offers
356 invaluable insights into tumor progression, adaptability, and heterogeneity across metastatic stages
357 in individual patients. The aggregation of CTCs from different patients within the central region
358 of the UMAP signifies that CTCs exhibit similar transcriptomic profiles despite their origin.
359 Importantly, the significant expression of AST factors not only in CTCs but also in their
360 intermediate solid tumor counterparts from pseudotime analysis indicate that anchorage plasticity
361 from AST to SAT is an adaptive and continuous process throughout the metastatic cascade. The
362 consistency of these trends across tumor subtypes and metastatic locations underscores the broad
363 significance of AST factors as theragnostic biomarkers of metastasis. To elucidate the role of

364 tumor microenvironment as an upstream mediator of AST factors, the spatiotemporal expression
365 patterns of AST factors using matched longitudinal specimens warrants further investigation.

366 Our study provides the rationale for clinical implementation of therapeutic strategies that
367 target AST factors and related mechanisms. For example, therapies designed to inhibit the
368 transition from adherent-to-suspension states, referred to as anti-disseminating agents, could
369 potentially be used as neoadjuvant therapies or alone to impede the initial detachment of cancer
370 cells from the primary tumor, thereby reducing the number of CTCs and the likelihood of
371 metastatic spread. Conversely, strategies that prevent the reattachment of CTCs at secondary sites
372 could hinder metastatic colonization, offering a two-pronged approach to tackle metastasis. A
373 deeper exploration into the genetic and epigenetic regulation of AST factors could yield additional
374 mechanistic insights into ASP. Understanding how AST factors are modulated during different
375 stages of metastasis, and the interplay between ASP and other forms of cellular plasticity, such as
376 EMP, warrants further investigation to delineate how these processes collectively contribute to the
377 completion of metastasis.

378 Together, our findings highlight the unprecedented role of ASP in breast cancer metastasis.
379 ASP provides a novel theoretical basis in cancer metastasis and suggests AST factors as promising
380 therapeutic targets to tackle the metastatic spread of solid tumor cells. Clinically, moving beyond
381 the primary tumor-centric point-of-view, our data expand the prevailing cancer treatment paradigm
382 toward direct intervention within the metastatic processes. The availability of cell-based platforms
383 that measure ASP efficiency and multi-omics database of matched longitudinal patient samples
384 could facilitate future research opportunities, including individualized metastasis prediction
385 models, hence augmenting the potential for developing effective anti-metastatic therapies [25].
386

387 ## METHODS

388 ### DNA constructs

389 AST genes were tagged with V5 and subcloned into the pENTR4 vector (Addgene, 17425 and
390 17423) using standard molecular cloning techniques. The resulting subcloned vectors were then
391 recombined with the destination vector pLentiCMV (Addgene, 17293) using LR recombinase
392 (Invitrogen, 1179019), generating the final lentiviral expression vectors.

393

394 ### Cell culture

395 Cells were maintained in a 37 °C humidified incubator with 5% CO_2. HEK293T, MCF7, HS578T
396 and MDA-MB-231 cells were cultured in DMEM (Hyclone, SH30022.01). BT549 cells were
397 cultured in RPMI (Hyclone, SH30027.01). Culture media were supplemented with 10% FBS
398 (Hyclone, SV30207.02) and 1% penicillin/streptomycin (Invitrogen, 15140122).

399

400 ### Cell competition assay

401 Cell competition assays were performed using MDA-MB-231, MCF7, BT549, and HS578T cells,
402 with each cell line cultured in its own respective growth media. For the assay, the cells were seeded
403 on normal plates at 80% confluency on the first day and then maintained for 3 days without any
404 media changes. After 3 days, the cells surpass 100% confluency, resulting in very high cell density.
405 After the old media were replaced with fresh media, the cells were cultured for an additional 3
406 days at 100% confluency. We noticed MDA-MB-231 cells began to round up and detach from the
407 plate beginning on the second day after the media change. By the third day, we observed a higher
408 number of CTC-like cells. These detached CTC-like cells were harvested by collecting the media,
409 followed by centrifugation to isolate the cells. For MCF7 cells, despite the media change, the cells

410 began to die after 3 days. Although BT549 and HS578T cells did not exhibit cell death, they did
411 cease proliferating.
412
413 **Viral infection**
414 To generate lentiviral particles, HEK293T cells were transfected with plasmids encoding pMD2G
415 and psPAX2, along with the lentiviral vectors containing the desired constructs. Transfections
416 were performed using Polyplus Reagent (Merck) according to the manufacturer's protocol. At 48
417 hours post-transfection, media containing the viral particles were harvested from the transfected
418 cells. The harvested media were then filtered through a 0.45 μm filter to remove cellular debris.
419 To enhance infection efficiency, the filtered media were supplemented with 8 mg/ml polybrene.
420 The transduced cells were infected with the lentiviral particles by incubating them with the filtered
421 media. After 24 hours of infection, the media were changed, and the cells were incubated for
422 another 24 hours. Then, transduced cells were selected using puromycin. The selection process
423 allowed for the enrichment of cells that successfully integrated the lentiviral vectors and expressed
424 the desired genes or markers.
425
426 **Cell viability assay**
427 *In vitro* cell viability was assessed using the CellTiter Glo® 2.0 cell viability assay (Promega,
428 G9241) and the LIVE/DEAD® cell imaging kit (ThermoFisher, R37601) according to their
429 manufacturers' protocols. For the suspension assay, cells were plated on Corning® Costar® Ultra-
430 Low Attachment Multiple-Well Plates (Merck, CLS3471).
431
432 **Quantitative real-time PCR analysis**

433 Cellular RNA samples were collected via RNA extraction using the RNeasy Plus mini kit
434 (QIAGEN, 74136). These RNA samples were then reverse transcribed into complementary DNA
435 (cDNA) using iScript reverse transcriptase (Bio-Rad, 1708891). The KAPA SYBR FAST qPCR
436 kit (Kapa Biosystems, KK4605) and the 7300 real-time PCR system (Applied Biosystems) were
437 used for quantitative real-time PCR (qRT-PCR). The following primer sequences were used for
438 qPCR: IKZF1, 5'-TTTCAGGGAAGGAAAGCCCC-3' (forward) and 5'-
439 CTCCGCACATTCTTCCCCAT-3' (reverse); NFE2, 5'-ACAGCTGTCCACTTCAGAGC-3'
440 (forward) and 5'-TGAGCAGGGGCAGTAAGTTG-3' (reverse); IRF8, 5'-
441 AGCATGTTCCGGATCCCTTG-3' (forward) and 5'-CGGTCCGTCACTTCCTCAAA-3'
442 (reverse); and ACTB, 5'-GCCGACAGGATGCAGAAGGAGATCA-3'(forward) and 5'-
443 AAGCATTTGCGGTGGACGATGGA-3'(reverse).
444

445 **siRNA transfection**

446 A transfection mix was prepared by combining 100 µl of Opti-MEM™ medium (ThermoFisher,
447 #31985070), 12 µl of RNAi Max transfection reagent (Invitrogen, 13778150), and 2 µl of 20 µM
448 siRNA. The following siRNAs were used for transfection: non-silencing (NS) siRNA (Dharmacon
449 siGENOME non-targeting control pool #D-001206-13-200), siIKZF1 (Dharmacon siGENOME
450 SMARTPool #M-019092-01-0010), siNFE2 (Dharmacon siGENOME SMARTPool #M-010049-
451 00-0010), siIRF8 (Dharmacon siGENOME SMARTPool #M-011699-01-0010), and siPOU2F2
452 (Dharmacon siGENOME SMARTPool #M-019690-01-0010).
453

454 **Mouse model experiments**

455 All animal experiment protocols in this study underwent a thorough review and received approval
456 from the Yonsei University Institutional Animal Care and Use Committee (IACUC). All

457 procedures involving animals adhered to the Guidelines for the Care and Use of Laboratory
458 Animals. The NOD SCID Gamma (NSG) mice used for orthotopic injection experiments were
459 obtained from JA Bio. For the orthotopic mouse model experiments, mammary fat pads of 7-week-
460 old female NSG mice were orthotopically injected with $1x10^6$ MCF7, BT549, HS578T, or MDA-
461 MB-231 cells. For the mouse tail vein injection experiments, the tail veins of 7-week-old female
462 NSG mice were injected with $1x10^5$ MDA-MB-231 derivative LM2 cells. At week 4, the mice
463 were euthanized for bioluminescence imaging using the In Vivo Imaging Spectrum (IVIS) device
464 (PerkinElmer, CLS136331 IVIS Lumina LT Inst, Series III, 120 V). All *in vivo* experiments were
465 carried out using mice that had received the same treatment. The NSG mice used in these
466 experiments possessed an identical genotype and genetic background.
467

468 **Statistical analyses**

469 All quantitative data were obtained from at least three independent biological replicates. Data are
470 presented as means ± standard deviation (SD) unless otherwise noted in the figure legends.
471 Statistical differences between two groups were examined using two-tailed, unpaired Student's t-
472 tests or one-way analysis of variance (ANOVA) with Bonferroni corrections for multiple
473 comparisons. Statistical tests were performed using the GraphPad Prism 9.0 software (GraphPad
474 Software, CA, USA). Two-sided p-values of less than 0.05 were considered significant. No
475 statistical methods were used to predetermine sample size. Sample size was based on previous
476 experience with experimental variability. Blinding was performed wherever possible during all
477 sample analysis by coding sample identity during data collection and having the analysis
478 performed by an observer without knowledge of or access to the experimental conditions.
479

480 **Bioinformatics of primary tumor cells, CTCs, and metastatic cancer cells**

481 The illumina outputs for human samples were mapped to the human reference genome (GRCh38)
482 using Cell Ranger 7.1.0 (10X Genomics). Gene-wise read counts for genes with at least 500 reads
483 were exported from Cell Ranger to the Matrix Market format and imported into R with Seurat's
484 Read10X function. An average of > 135 million reads from > 13,000 cells were obtained for each
485 sample. Each 10X library was individually checked for quality, and the cells were filtered
486 according to the same criteria used in our previous study to ensure good gene coverage [4]. After
487 quality control filtering, a total of 310,189 cells remained, with 69,612 cells from the primary
488 tumor site, 171,504 cells from the blood, and 79,073 cells from the metastatic site (**Table 1**).
489 Samples were combined via an algorithm implemented in Seurat. The default Seurat function
490 settings were used, and 1:20 principal component dimensions were used for all dimension
491 reduction and integration steps. The cluster resolutions were set to 0.5, unless otherwise stated.
492 The RunUMAP random seed was set to 1,000 to ensure reproducibility. Marker genes for cell
493 clusters were identified using Seurat's FindMarkers function with the default settings. Cell type
494 annotation was performed using the SingleR package (v2.6.0) with the HumanProteinAtlas
495 database from the celldex package (v1.14.0). Cells co-expressing EPCAM and cytokeratins such
496 as KRT5, KRT8, KRT9, KRT17, or KRT18 were designated as cancer cells. A total of 54,867
497 cells were used for the analysis, including 26,227 cells from the primary tumor site, 50 cells from
498 the blood, and 28,590 cells from metastatic sites (**Table 1**). The cells designated as cancer cells
499 were subsequently extracted and reanalyzed beginning with the normalization process. DEGs were
500 selected with thresholds for the FDR corrected p-value < 0.001 and an absolute $\log_2$ fold change
501 ≥ 1. GO analysis was performed using the gseGO function from clusterProfiler (v3.0.4). GSEA
502 plots were generated from the DEG data using the gseaplot function. Pseudotime analysis was
503 performed using the monocle package (v3.0) with normalized data, UMAP coordinates, and cluster

information obtained from the initial Seurat analysis. The calculation of gene set scores along pseudotime was conducted for each cell using the AddModuleScore function in Seurat. All plots were exported to the PDF format using R and their dimensions were adjusted in Illustrator.

Declarations

Ethical approval

Ethical approval for the use of human subjects was obtained from the Institutional Review Board of Gangnam Severance Hospital, Yonsei University, Seoul, Republic of Korea (3-2021-0236) in compliance with the ethical guidelines of the 1975 Declaration of Helsinki, and informed written consent was obtained from each patient. Collection of human breast cancer samples were obtained from consenting patients in accordance with guidelines and regulations approved by the Institutional Review Board of Gangnam Severance Hospital, Yonsei University Health System (3-2021-0236). The animal experiment protocols were reviewed and approved by the Yonsei University Institutional Animal Care and Use Committee (IACUC).

Competing interests

The authors declare that they have no conflict of interest.

Fundings and acknowledgments

This work was supported by grants from the National Research Foundation of Korea (2020M3F7A1094077, 2020M3F7A1094089, 2021R1A2C1010828, 2020R1A4A1019063, 2018R1C1B6004301 to H.W.P., to H.Y.G.,), , by the Brain Korea 21 FOUR Program (to H.D.H., Y.S., H.L., B.J.H., W.Y.P., J.O., and D.K.L.)

Authors' contributions

H.D.H., Y.S., and J.H.K. performed most of the experiments. H.L., B.J.H., W.Y.P. performed drug treatment and imaging. J.O., and D.K.L. performed transcriptome analyses. S.P. and J.C.

550 performed CTC isolation and scRNAseq. J.J., H.Y.G., and H.W.P. designed the study and wrote

551 the manuscript.

552 **References**

553 1. Chaffer CL, Weinberg RA: A perspective on cancer cell metastasis. *Science* 2011,
554 331:1559-1564.

555 2. Nguyen DX, Bos PD, Massague J: Metastasis: from dissemination to organ-specific
556 colonization. *Nat Rev Cancer* 2009, 9:274-284.

557 3. Marabitti V, Caruana I, Nazio F: Should I stay or should I go? Spatio-temporal control of
558 cellular anchorage by hematopoietic factors orchestrates tumor metastatic cascade. *Mol*
559 *Cancer* 2023, 22:149.

560 4. Huh HD, Sub Y, Oh J, Kim YE, Lee JY, Kim HR, Lee S, Lee H, Pak S, Amos SE, et al:
561 Reprogramming anchorage dependency by adherent-to-suspension transition promotes
562 metastatic dissemination. *Mol Cancer* 2023, 22:63.

563 5. Huh HD, Park HW: Emerging paradigms in cancer cell plasticity. *BMB Rep* 2024, 57:273-
564 280.

565 6. Lee JY, Huh HD, Lee DK, Park SY, Shin JE, Gee HY, Park HW: Reprogramming
566 anchorage dependency to develop cell lines for recombinant protein expression. *Biotechnol*
567 *J* 2024, 19:e2400104.

568 7. Massague J, Obenauf AC: Metastatic colonization by circulating tumour cells. *Nature*
569 2016, 529:298-306.

570 8. Lee DK, Oh J, Park HW, Gee HY: Anchorage Dependence and Cancer Metastasis. *J*
571 *Korean Med Sci* 2024, 39:e156.

572 9. Weiswald LB, Bellet D, Dangles-Marie V: Spherical cancer models in tumor biology.
573 *Neoplasia* 2015, 17:1-15.

574 10. Puck TT, Marcus PI, Cieciura SJ: Clonal growth of mammalian cells in vitro; growth
575 characteristics of colonies from single HeLa cells with and without a feeder layer. *J Exp*
576 *Med* 1956, 103:273-283.
577 11. Borowicz S, Van Scoyk M, Avasarala S, Karuppusamy Rathinam MK, Tauler J, Bikkavilli
578 RK, Winn RA: The soft agar colony formation assay. *J Vis Exp* 2014:e51998.
579 12. Woods NT, Yamaguchi H, Lee FY, Bhalla KN, Wang HG: Anoikis, initiated by Mcl-1
580 degradation and Bim induction, is deregulated during oncogenesis. *Cancer Res* 2007,
581 67:10744-10752.
582 13. Koch C, Kuske A, Joosse SA, Yigit G, Sflomos G, Thaler S, Smit DJ, Werner S, Borgmann
583 K, Gartner S, et al: Characterization of circulating breast cancer cells with tumorigenic and
584 metastatic capacity. *EMBO Mol Med* 2020, 12:e11908.
585 14. Sun YF, Wu L, Liu SP, Jiang MM, Hu B, Zhou KQ, Guo W, Xu Y, Zhong Y, Zhou XR,
586 et al: Dissecting spatial heterogeneity and the immune-evasion mechanism of CTCs by
587 single-cell RNA-seq in hepatocellular carcinoma. *Nat Commun* 2021, 12:4091.
588 15. Ebright RY, Lee S, Wittner BS, Niederhoffer KL, Nicholson BT, Bardia A, Truesdell S,
589 Wiley DF, Wesley B, Li S, et al: Deregulation of ribosomal protein expression and
590 translation promotes breast cancer metastasis. *Science* 2020, 367:1468-1473.
591 16. Garcia-Recio S, Hinoue T, Wheeler GL, Kelly BJ, Garrido-Castro AC, Pascual T, De
592 Cubas AA, Xia Y, Felsheim BM, McClure MB, et al: Multiomics in primary and metastatic
593 breast tumors from the AURORA US network finds microenvironment and epigenetic
594 drivers of metastasis. *Nat Cancer* 2023, 4:128-147.

595 17. Turajlic S, Xu H, Litchfield K, Rowan A, Chambers T, Lopez JI, Nicol D, O'Brien T,
596 Larkin J, Horswell S, et al: Tracking Cancer Evolution Reveals Constrained Routes to
597 Metastases: TRACERx Renal. *Cell* 2018, 173:581-594 e512.
598 18. Jin X, Demere Z, Nair K, Ali A, Ferraro GB, Natoli T, Deik A, Petronio L, Tang AA, Zhu
599 C, et al: A metastasis map of human cancer cell lines. *Nature* 2020, 588:331-336.
600 19. Minn AJ, Gupta GP, Siegel PM, Bos PD, Shu W, Giri DD, Viale A, Olshen AB, Gerald
601 WL, Massague J: Genes that mediate breast cancer metastasis to lung. *Nature* 2005,
602 436:518-524.
603 20. Lee SJ, Lee CH, Choi SH, Ahn SH, Son BH, Lee JW, Yu JH, Kwon NJ, Lee WC, Yang
604 KS, et al: Evaluation of a novel approach to circulating tumor cell isolation for cancer gene
605 panel analysis in patients with breast cancer. *Oncol Lett* 2017, 13:3025-3031.
606 21. Li F, Liang H, You H, Xiao J, Xia H, Chen X, Huang M, Cheng Z, Yang C, Liu W, et al:
607 Targeting HECTD3-IKKα axis inhibits inflammation-related metastasis. *Signal Transduct*
608 *Target Ther* 2022, 7:264.
609 22. Yuan S, Norgard RJ, Stanger BZ: Cellular Plasticity in Cancer. *Cancer Discov* 2019,
610 9:837-851.
611 23. Fanelli GN, Naccarato AG, Scatena C: Recent Advances in Cancer Plasticity: Cellular
612 Mechanisms, Surveillance Strategies, and Therapeutic Optimization. *Front Oncol* 2020,
613 10:569.
614 24. Akhmetkaliyev A, Alibrahim N, Shafiee D, Tulchinsky E: EMT/MET plasticity in cancer
615 and Go-or-Grow decisions in quiescence: the two sides of the same coin? *Mol Cancer*
616 2023, 22:90.

617 25. Anderson RL, Balasas T, Callaghan J, Coombes RC, Evans J, Hall JA, Kinrade S, Jones
618 D, Jones PS, Jones R, et al: A framework for the development of effective anti-metastatic
619 agents. *Nat Rev Clin Oncol* 2019, 16:185-204.
620

621 **Figure 1. Cell competiton orchestrates spontaneous detachment of CTC-like cells driven**

622 **by AST factors expression *in vitro***

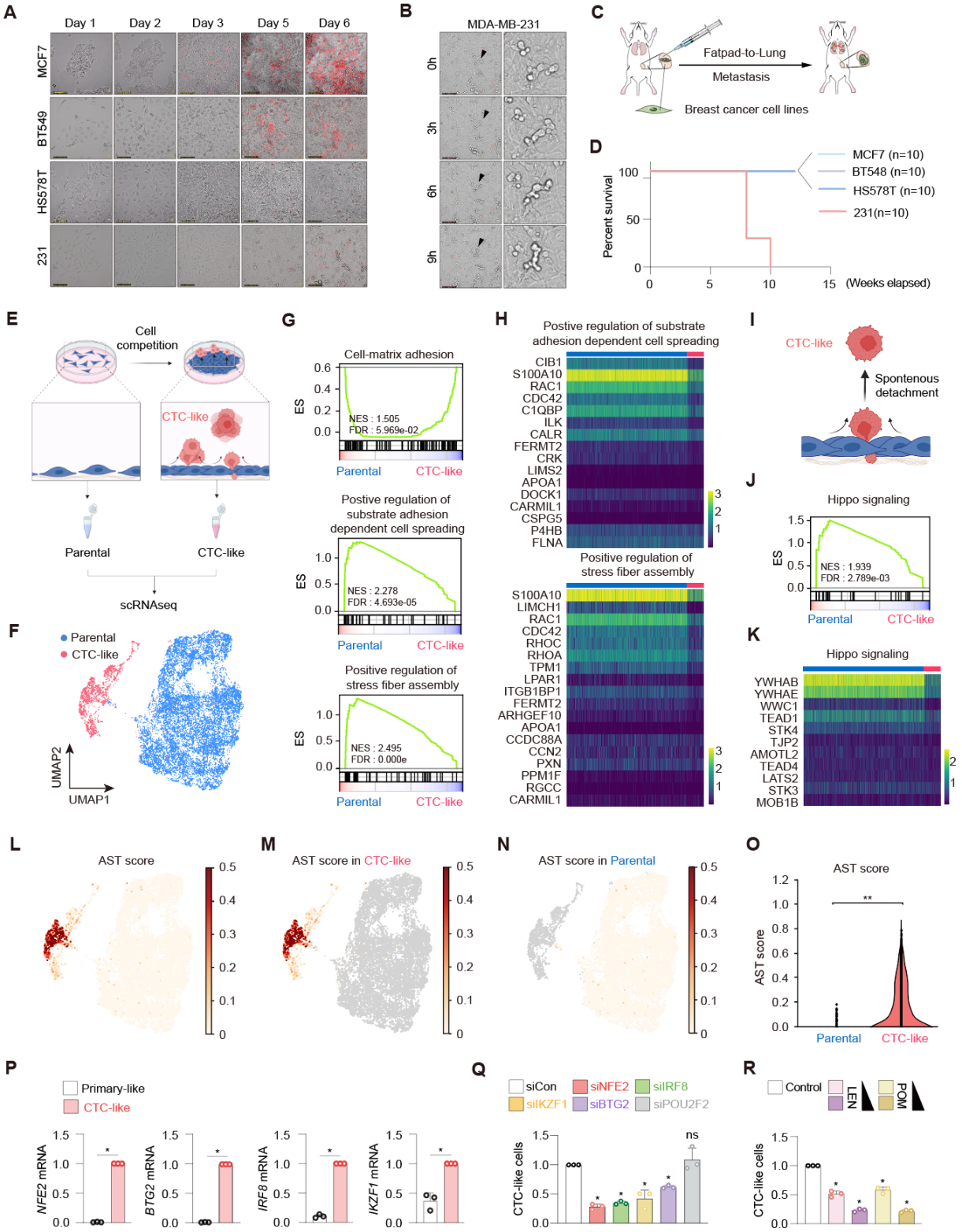

623

624 **A**, Representative fluorescence images MCF7, BT549, Hs578T and MDA-MB-231 cells stained
625 for viability with propidium iodide. Red, dead. Scale bars, 100 μm. **B**, Time-lapse microscopy
626 images showing spontaneous cell detachment of MDA-MB-231 cells in the dissemination assay.
627 **C**, Schematic overview of mammary fat pad xenografts of 4 different breast cancer cell lines. **D**,
628 Kaplan-Meier survival plot showing the survival rates of mice injected with MCF7, BT549,
629 Hs578T, or MDA-MB-231 cells. **E**, Schematic overview of the isolation and scRNA-seq analysis
630 of parental cells and circulating tumor cells-like (CTC-like) cells from cell competition. **F**,
631 Uniform manifold approximation and projection (UMAP) of scRNA-seq cells (13,918 cells)
632 colored by parnetal (blue) and CTC-like cells (red). **G**, Gene set enrichment analysis (GSEA)
633 results for cell-matrix adhesion, positive regulation of substrate adhesion dependent cell spreading,
634 and positive regulation of stress fiber assembly gene sets within CTC-like cells. **H**, Heatmap
635 showing differentially expressed genes (DEGs). DEGs were identified based on gene set enriched
636 in GSEA result in (G). **I**, Schematic overview of spontaneously detached CTC-like cells from
637 parental cells. **J**, Gene set enrichment analysis (GSEA) results for hippo signaling gene sets within
638 CTC-like cells. **K**, Heatmap showing differentially expressed genes (DEGs). DEGs were identified
639 based on gene set enriched in GSEA result in (K). **L**, UMAP of scRNA-seq cells showing AST
640 score, calculated with Scnapy's score_genes function, which reflects the normalized difference in
641 mean expression between AST genes (IKZF1, NFE2, BTG2, and IRF8) and control genes. **M**,
642 UMAP of scRNA-seq cells showing AST score in CTC-like cells. **N**, UMAP of scRNA-seq cells
643 showing AST score in parental cells. **P,** Representative images of CTC-like MDA-MB-231 cell
644 morphology and quantitative real-time PCR analysis of AST factor transcript levels in CTC-like
645 cells. **Q**, The number of CTC-like cells for MDA-MB-231 cells following siRNA-mediated AST

646 factor depletion. N = 3. **R**, The number of CTC-like cells for MDA-MB-231 cells following
647 treatment with lenalidomide or pomalidomide. N = 3.
648
649
650
651
652
653
654
655
656
657
658
659
660
661
662
663
664
665
666
667
668

669

670 **Figure 2. CTC-like cells reflect CTCs characterized by AST factor expression.**

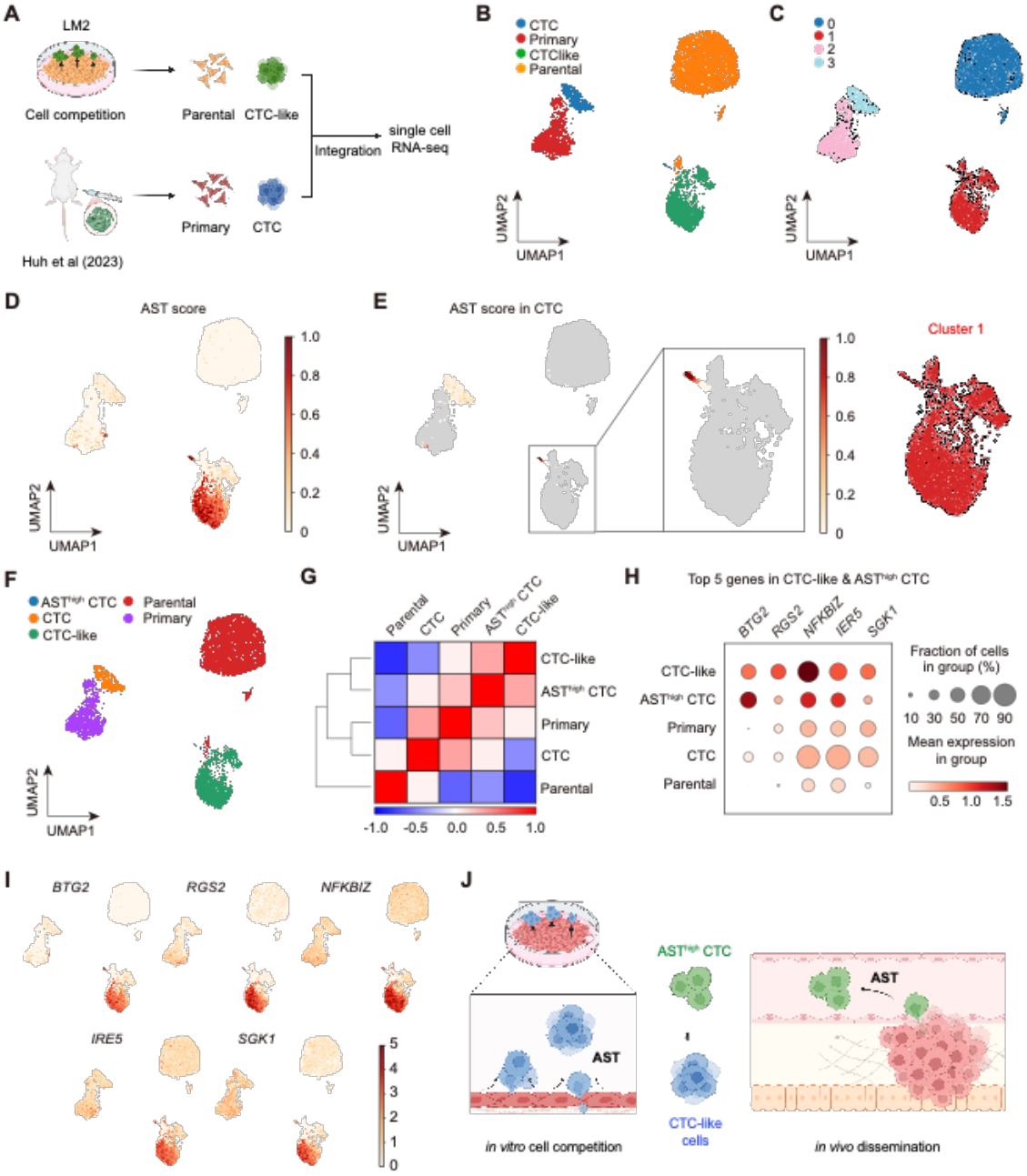

671

672 **A,** Schematic overview illustrating the integration of scRNA-seq analysis of in vitro cell

673 competition data (parental cells and CTC-like cells) with in vivo orthotopic fatpad-to-lung

674 metastasis data (primary tumor and circulating tumor cells, CTCs). **B**, Uniform manifold
675 approximation and projection (UMAP) of scRNA-seq cells (26,571 cells) colored by samples
676 (CTCs, primary tumor, CTC-like cells and parental cells) **C**, Uniform manifold approximation and
677 projection (UMAP) of scRNA-seq cells (26,571 cells) colored by leiden algorithm. **D**, Uniform
678 manifold approximation and projection (UMAP) of scRNA-seq cells (26,571 cells) colored by
679 normalized AST score, calculated with Scnapy's score_genes function, which reflects the
680 normalized difference in mean expression between AST genes (IKZF1, NFE2, BTG2, and IRF8)
681 and control genes. **E**, Uniform manifold approximation and projection (UMAP) of scRNA-seq
682 cells (26,571 cells) colored by normalized AST score in CTCs. **F**, Uniform manifold
683 approximation and projection (UMAP) of scRNA-seq cells (26,571 cells) colored by annotated
684 cell type (AST^{high} CTCs, CTC-like, CTCs, primary tumor, and parental cells). **G**, Pearson
685 correlation analysis showing the transcriptional correation between annotated cell types in **F**. **H**,
686 Dot plots showing the expression level of five top genes that is highly expressed in AST^{high} CTCs
687 and CTC-like in annotated cell types in **F**. **I**, Uniform manifold approximation and projection
688 (UMAP) of scRNA-seq cells (26,571 cells) colored by normalized expression of 5 top genes in **H**.
689 **J**, Schematic model illustrating that in vitro CTC-like cells generated thorugh cell competition
690 recapitulate in vivo AST^{high} CTCs.
691
692
693
694
695
696
697

Figure 3. CTC-like cells and CTCs confer anchorage dependency plasticity accompanied by AST factors oscillation.

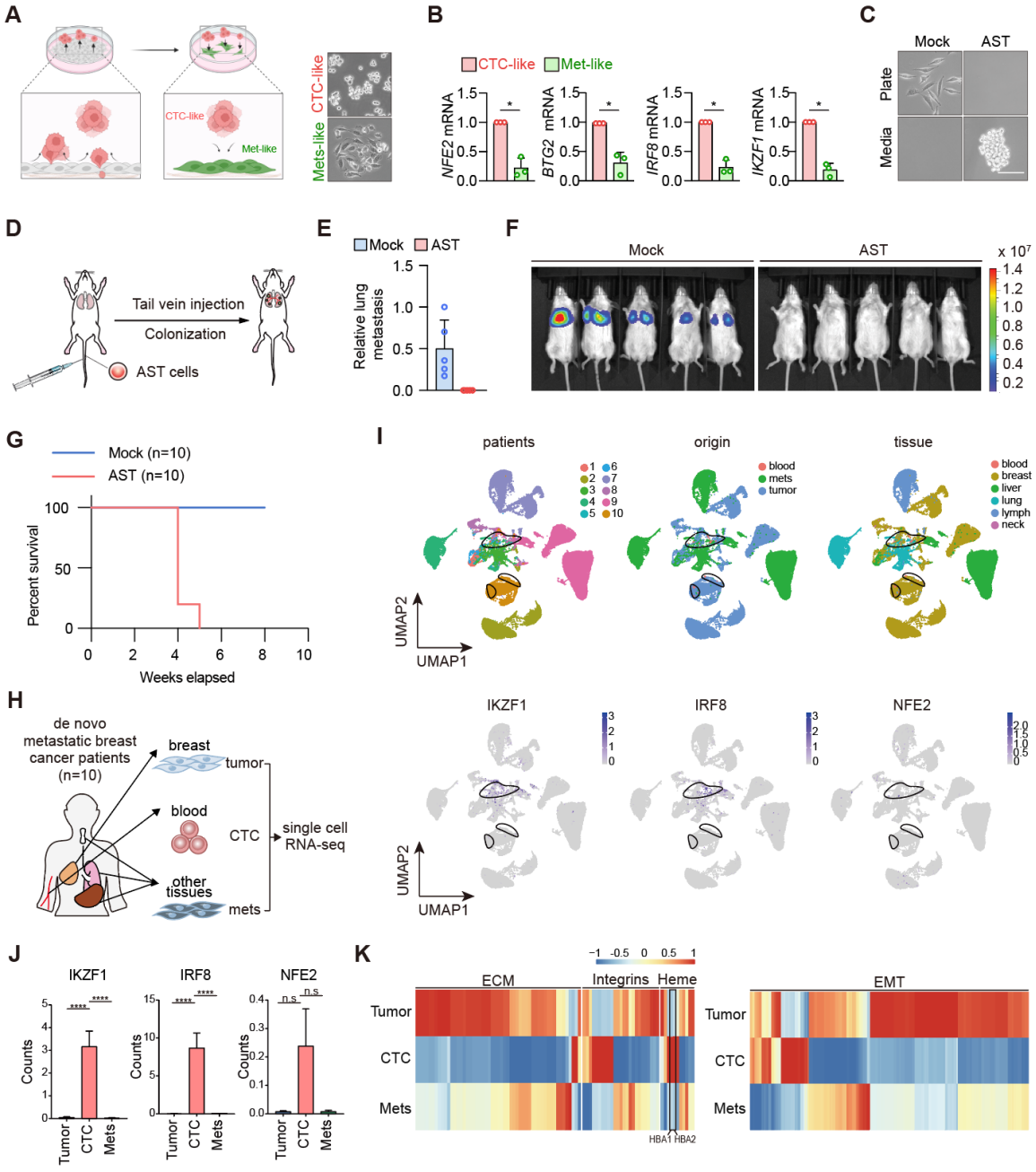

A, Schematic overview of CTC-like cells and mets-like cells, and representative images of re-attached MDA-MB-231 cell (met-like cells) morphology. **B**, Quantitative real-time PCR analysis of AST factor transcript levels in met-like cells compared to CTC-like cells. **C**, Representative

704 images of MDA-MB-231 derivates LM2-mock or AST cell (LM2 cells expressing AST factors)
705 morphology on a culture plate or in media. **D**, Schematic overview of tail vein injections with
706 LM2-mock or AST cells. **E**, Bioluminescence images of lung metastases after LM2 tail vein
707 injections. **F**, Lung metastases quantified by lung bioluminescence intensity for mock versus AST
708 cells. **G**, Kaplan-Meier survival plot showing the survival rates of mice injected with mock or
709 3AST cells. N = 10. **H,** Schematic overview of the isolation and scRNA-seq analysis of primary
710 tumor cells, circulating tumor cells (CTCs), and metastatic tumor cells from de novo metastatic
711 breast cancer patients (n = 10). CTCs were isolated using HDM chips. **I,** Uniform manifold
712 approximation and projection (UMAP) of scRNA-seq cells (n = 10; 54,866 cells) colored by
713 patient, origin, tissue, and normalized gene expression of the AST factors IKZF1, IRF8, and NFE2.
714 Black border lines, area in which the CTCs are located. **J,** Dynamite plots showing the expression
715 of (left) IKZF1, (middle) IRF8, and (right) NFE2 in primary tumor cells, CTCs, and metastatic
716 tumor cells. ****, $P < 0.0001$; n.s, not significant ($P > 0.05$). **K**, Heatmaps showing normalized
717 expression of four gene sets—ECM, integrins, antioxidant defense genes, and EMT-related
718 genes—in primary tumors, CTCs, and metastases. The average normalized expression values for
719 cells within each group are displayed as scaled values. Black-bordered box, HBA1 and HBA2.
720

721 **Figure 4. AST plasticity in matched single cell RNA-seq samples from *de novo* breast**

722 **cancer patients.**

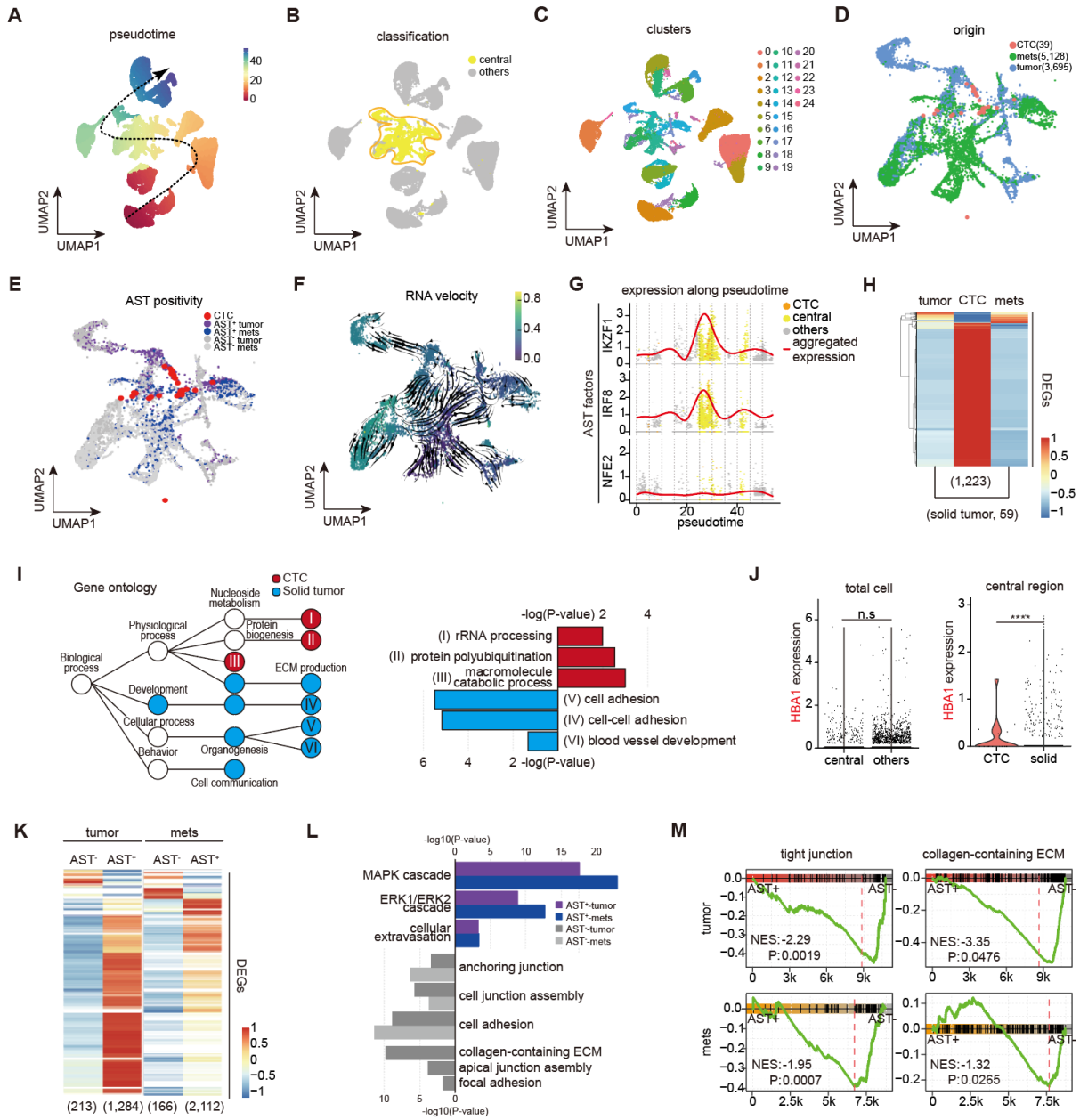

723

724 **A-C**, UMAP plot showing pseudotime (A), a division between the central region containing

725 complex clusters with CTCs and others (B), and clusters calculated at a resolution of 0.5 (C).

726 Dotted arrow, flow of pseudotime for the normalized gene expression of the AST factors IKZF1,

727 IRF8, and NFE2. **D-F**, UMAP of the central region colored according to origin (D) , AST positivity

728 (E), and RNA velocity (F). **G**, Pseudotime expression plots showing AST factors. X-axis,
729 pseudotime; y-axis, expression levels; gray dots, others; yellow dots, central region; orange dots,
730 CTCs; red line, linear expression trend using generalized additive modeling (GAM). **H**, Heatmap
731 showing differentially expressed genes (DEGs). DEGs were identified based on comparisons
732 between solid tumor cells and CTCs within the central region and selected with a threshold p-value
733 < 0.05. There were 1,223 CTC DEGs and 59 solid tumor DEGs. **I**, Gene ontology tree showing
734 the CTC-specific gene set and the solid tumor-specific gene set with a bar plot showing the gene
735 names and the p-values corresponding to the circles marked with roman numerals. Colored circles,
736 statistically significant, FDR corrected $P < 0.01$. **J**, Violin plots with dots showing HBA1
737 expression. The first plot compares the central region with other groups, while the second plot
738 compares CTCs with solid tumor cells within the central region. Yellow, central region; gray,
739 others; orange, CTCs within the central region; turquoise, solid tumor cells within the central
740 region; ****, $P < 0.0001$; n.s, not significant ($P > 0.05$). **K**, Heatmap showing DEGs. In a
741 comparison of cells with and without AST factor expression in both primary and metastatic tumors,
742 the DEG thresholds were defined as an FDR corrected q-value < 0.001 and an absolute fold change
743 > 2. **L**, Bar plot showing ontology analysis results for the AST-positive and AST-negative gene
744 sets identified in (**K**). Purple bars, AST-positive gene sets in primary tumors; blue bars, AST-
745 positive gene sets in metastatic tumors; gray bars, AST-negative gene sets in primary tumors; light
746 gray bars, AST-negative gene sets in metastatic tumors. **M**, Gene set enrichment analysis (GSEA)
747 results for tight junction and collagen-containing ECM gene sets within both primary and
748 metastatic tumors.
749
750

751 **Supplementary Figure 1. The ability to generate AST factors-expressing CTC-like cells is**

752 **correlated with their metastatic capability.**

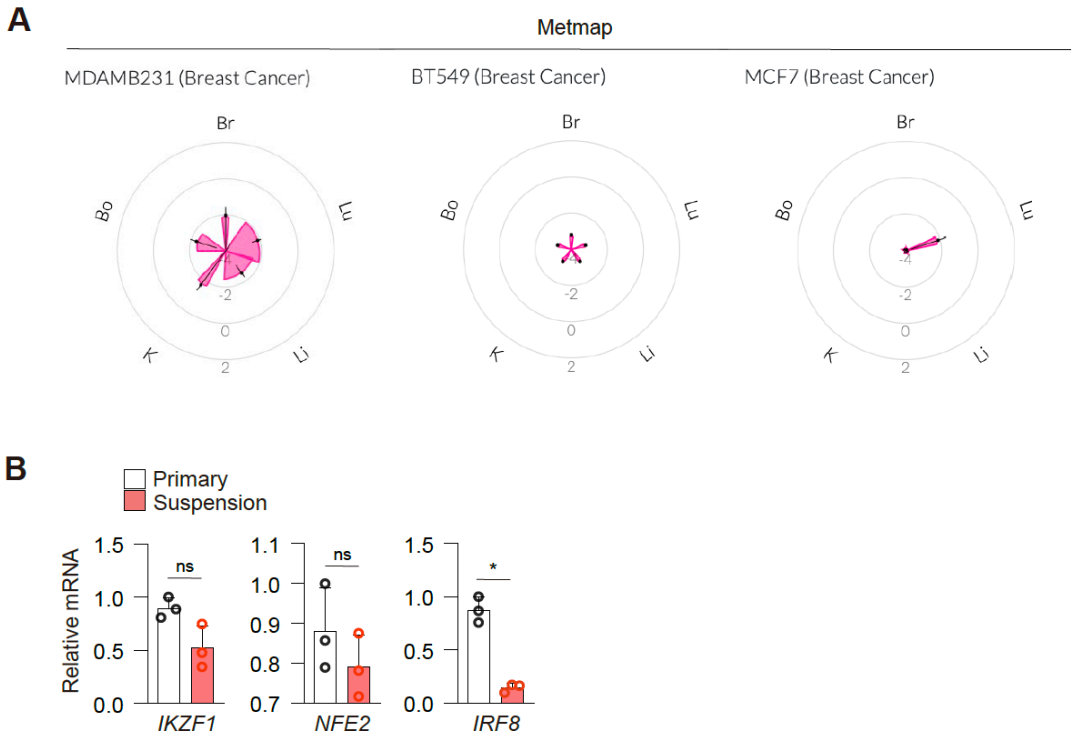

753

754 **A**, Petal plots showing the metastatic patterns of 3 breast cancer cell lines. Data for these plots

755 were obtained from Jin, X., *et al*. (https://depmap.org/metmap). **B**, Quantitative real-time PCR

756 analysis of AST factor transcript levels in cells harvested from suspension assay.

757 **Supplementary Figure 2. Comprehensive overview of single cell RNA sequencing**

758 **data from breast cancer patients.**

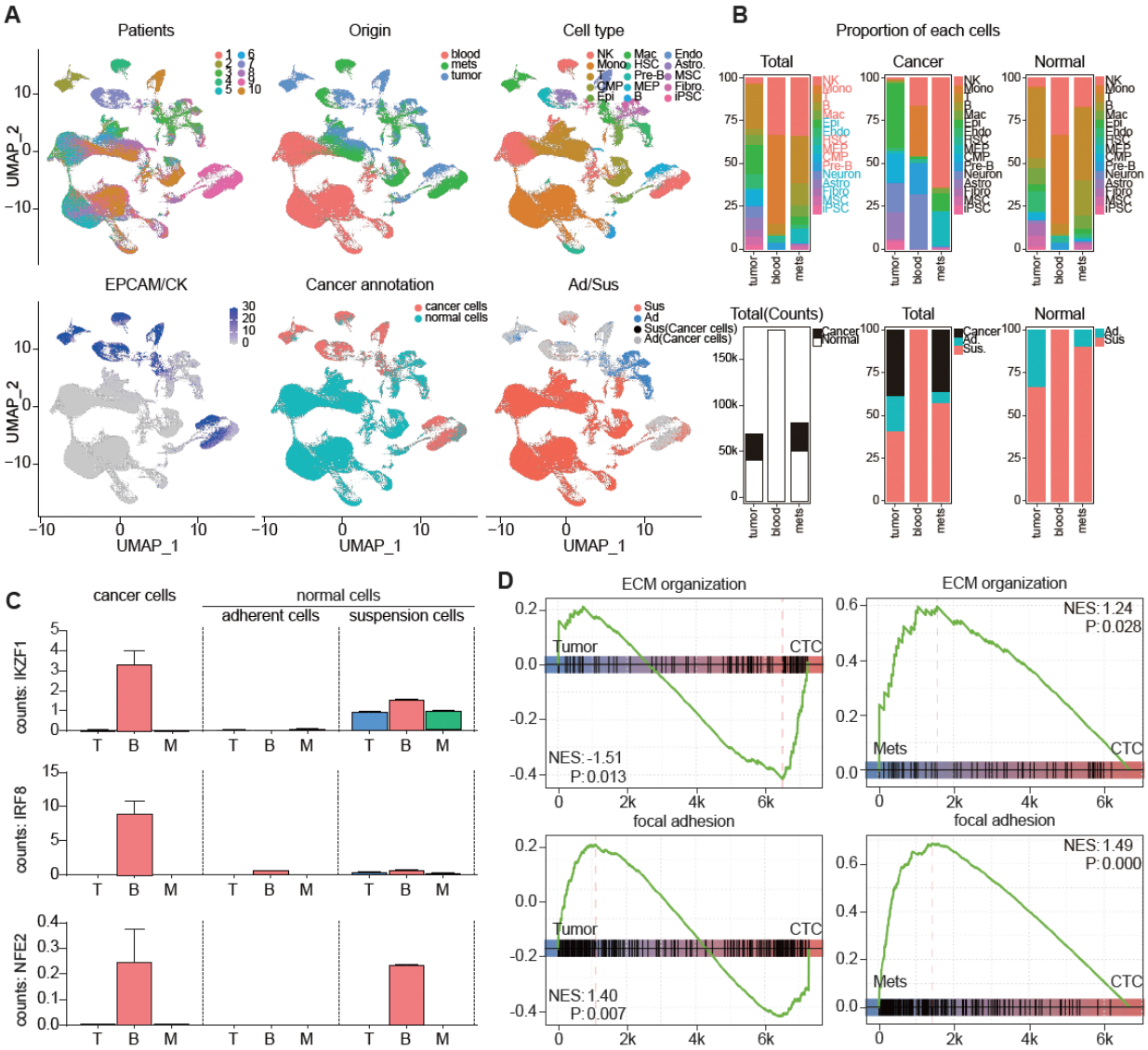

759

760 **A**, Uniform manifold approximation and projection (UMAP) of scRNA-seq cells (n = 316,539

761 cells) colored by patient, origin, cell type, normalized gene expression of cancer cell markers

762 (EPCAM, KRT5, KRT7, KRT8, KRT18, and KRT19), cancer/non-cancer annotation, and the

763 combined cancer/non-cancer and adherent/suspension annotation. **B**, Bar plots showing a

764 breakdown of cell type composition across tumor, blood, and metastasis samples. The first row

765 shows the proportion of various cell types in total cells, cancer cells, and normal cells. The
766 second row shows the proportion of cancer cells versus normal cells, adherent versus suspension
767 cells within cancer and normal cells, and adherent versus suspension cells within normal cells. **C**,
768 Dynamite plots depicting the expression of the AST factors IKZF1, IRF8, and NFE2 in cancer
769 cells from primary tumor, blood, and metastases, as well as normal cells split into adherent and
770 suspension states. **D**, Gene set enrichment analysis (GSEA) plots for focal adhesion and ECM
771 organization gene sets comparing CTCs to primary tumor or metastatic cells.

Supplementary Figure 3. Central region-specific cell populations and CTC–solid tumor divergence in scRNA sequencing data.

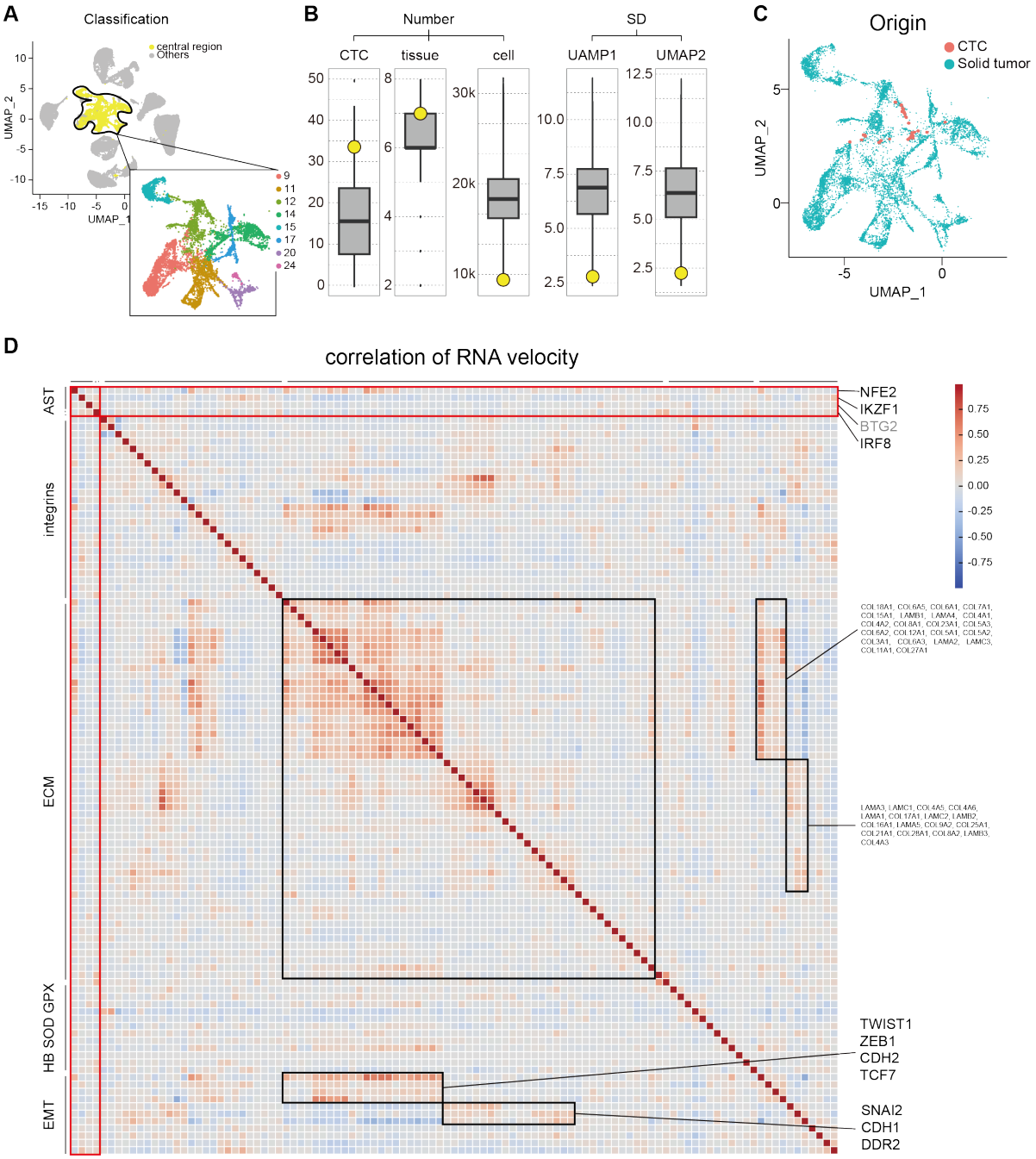

A, UMAP of cancer cells categorized into the central region and others. A magnified view of the central region is also shown to highlight its specific clusters. **B**, Boxplots of 1,081,575 cluster

778 combinations (binomial coefficient with n = 25, k-permutation = 8) presenting numbers of CTCs,
779 originating tissues, and total cells with standard deviations (SDs) for UMAP1 and UMAP2. Yellow
780 dot, selected cluster combination; CTCs, n = 34, 11.93%; originating tissues, n = 7, 8.83%; total
781 cells, n = 8,857, 99.31%; UMAP1 SD, 2.77, 90.69%; UMAP2 SD, 2.49, 0.36%. **C**, UMAP of cells
782 in the central region colored by anchorage status. Turquoise, solid tumor; orange, CTCs. **D**,
783 Heatmap of RNA velocity correlations among AST factor, ECM, integrin, superoxide resistance
784 genes, and EMT genes.

785 **Table S1. Overview of patient information used for single cell transcriptome analysis.**

Patient #	Metastasis tissue	Subtype	Total cell counts			Cancer cell counts		
			Tumor	Blood	Meta	Tumor	Blood	Meta
patient1	liver	Her2	1,746	7,209	2,411	659	2	1,033
patient2	neck	Luminal-B	13,246	9,499	-	9,198	-	-
patient3	lung	Her2	14,254	25,180	11,982	516	1	2,531
patient4	lung	Luminal-B	-	25,394	10,900	-	2	7,507
patient5	brain	Her2	1,569	19,071	-	82	1	-
patient6	lung	TNBC	3,612	13,166	5,034	324	1	19
patient7	lymph	Luminal-A	9,572	26,768	9,404	4,438	8	5,833
patient8	neck	TNBC	11,741	9,117	12,746	1,257	7	13
patient9	liver	Luminal-A	8,077	21,471	16,458	5,032	9	11,641
patient10	lymph	TNBC	5,795	14,629	10,138	4,721	19	13
			69,612	171,504	79,073	26,227	50	28,590

786

787 **Movie S1. Dissemination assay of various breast cancer cell lines**

788 **A**, Video of MCF7 cell proliferation in the dissemination assay.

789 **B**, Video of BT549 cell proliferation in the dissemination assay.

790 **C**, Video of HS578T cell proliferation in the dissemination assay.

791 **D**, Video of MDA-MB-231 cell proliferation in the dissemination assay.

792